Progress In Electromagnetics Research, Vol. 109, 191–209, 2010

ANGLE AND TIME OF ARRIVAL STATISTICS OF A THREE DIMENSIONAL GEOMETRICAL SCATTERING CHANNEL MODEL FOR INDOOR AND OUTDOOR PROPAGATION ENVIRONMENTS

M. Alsehaili

Department of Electrical and Computer Engineering
University of Manitoba, Winnipeg, Manitoba, R3T 5V6, Canada

S. Noghanian

Department of Electrical Engineering
School of Engineering and Mines
University of North Dakota, North Dakota 58202-7165, USA

A.-R. Sebak

Department of Electrical and Computer Engineering
Concordia University, Montreal, Quebec, H3G 1M8, Canada

D. A. Buchanan

Department of Electrical and Computer Engineering
University of Manitoba, Winnipeg, Manitoba, R3T 5V6, Canada

Abstract—In this paper, a three dimensional geometrical scattering channel model for indoor and outdoor wireless propagation environments is introduced. It is based on the assumption that the scatterers are distributed within a spheroid, in which the mobile station and base station are located at the spheroid's foci. This model captures both the spatial and temporal statistical distributions of the received multipath signals. Several angle of arrival and time of arrival probability density functions of the received multipath signals are provided in compact forms. The angle of arrival probability density functions are obtained in terms of both the azimuth and elevation angles. Numerical results are presented to illustrate and verify the derived expressions. To validate the model, it has been compared against some of the available two dimensional models and measured data.

Received 11 August 2010, Accepted 6 October 2010, Scheduled 21 October 2010
Corresponding author: Mohammad Alsehaili (msehaili@ee.umanitoba.ca).

1. INTRODUCTION

In wireless communication systems, the transmitted electromagnetic signals propagate between the transmitting and the receiving antennas along different paths, which result in a multipath propagation phenomenon. These multipath signals can limit the performance of wireless communication systems by introducing fading and/or intersymbol interference (ISI). In addition, the performance of wireless communication systems that employ antenna array is often limited by the spatial and temporal correlation of the received multipath signals. Therefore, the angular and temporal statistical distributions of the received multipath signals are significant factors in determining the performance of the radio link. These distributions can be obtained from measured channel data or from site specific propagation prediction data. However, normally, these data are unavailable and/or unapplicable. Therefore, channel models which are capable of predicting both the spatial and temporal characteristics of the received multipath signals are desirable for evaluating, analyzing and designing advanced wireless communication systems. Geometrical scattering channel models have been developed to describe the angle of arrival (AOA) and time of arrival (TOA) probability density functions (pdfs) of the received multipath signals. In the current literature, several two dimensional (2D) [1–13] and three dimensional (3D) [14–17] geometrical scattering channel models have been suggested for various types of wireless communication environments. For example, in macrocellular wireless environments, where the base station (BS) antennas are elevated and the scatterers are assumed to be located around only the mobile station (MS) antenna, many 2D and 3D geometric channel models have been developed [3–8, 11, 15, 17].

In outdoor picocellular and indoor wireless communication environments, the typical heights of the BS and MS antennas and the distance between them are both relatively short in comparison to outdoor macrocellular wireless environments. Therefore, scatterers such as roofs, walls, trees, doors, windows, the ground, etc., will be spread in a 3D space around and between both the BS and MS antennas. Therefore, it becomes more realistic to consider that incoming multipath signals take place within both the azimuth and elevation angles. In addition, several indoor and outdoor channel measurements [18–22] demonstrate that the angular spread of the received multipath signals are observed with a relatively wide range in elevation angle in contrast with the 2D models' assumptions. However, the published geometrical scattering channel models developed for such environments, i.e., outdoor picocellular and indoor environments,

are 2D models [1–3, 8, 9, 12, 13]. For example, Liberti and Rappaport in [1], developed the elliptical model by assuming that the scatterers are uniformly distributed inside an ellipse in which the BS and MS are assumed to be at its foci. Olenko et al. in [2], proposed a geometric channel model based on the assumption that the scatterers are distributed along circumferences of elevated ellipses, where the TOA variable is related to elevated BS antennas, but the AOA variable is based on distributing the scatterers on a 2D plane. In [3], Ertel and Reed developed a general method to derive the AOA and TOA pdfs for the circular model [1] and elliptical model [3] as seen from both the MS and BS. Jiang and Tan in [8], proposed a circular channel model in which the scatterers are randomly distributed according to an arbitrary scatterer density around the BS within a circle that includes the MS. In [9] Noor et al. generalized the elliptical channel model for an arbitrary distribution of scatterers at the MS and/or at the BS. Chen et al. in [12] proposed a geometrical scattering channel model for radio propagation in rectangular office buildings where the scatterers are assumed to be randomly distributed as arrays of thin strips. In [13], Chen et al. developed a geometrical scattering channel model to describe radio propagation in an indoor environment with directional antennas, where Von Mises function was used to describe the beam shapes. However, 2D models are only capable of providing the azimuthal angular distribution information of the received multipath signals, because the transmitted signals are assumed to propagate on the horizontal plane, i.e., at elevation angle $\theta = 90°$.

In this paper, a 3D geometrical scattering channel model has been developed for outdoor picocellular and indoor wireless communication environments, whereas currently only 2D models are available in literature. The model incorporates both the spatial and temporal statistical distributions of the received multipath signals. The spatial statistical distributions are expressed in terms of both the azimuth and elevation angles. Expressions for the AOA and TOA pdfs of the received multipath signals are provided in compact forms. The paper's organization is as follows. A description and formulation of the 3D model is given in Section 2. The derivation of the AOA and TOA pdfs of the multipath signals are provided in Section 3. To illustrate and verify the developed 3D model, several numerical results and comparisons are presented in Section 4. A conclusion is given in Section 5.

2. CHANNEL MODEL DESCRIPTION

The following assumptions have been used, which are commonly applied in literature for geometrical scattering channel techniques.

- The propagation between the BS and the MS is assumed to take place via a single scattering from an intervening obstacle. Without the loss of generality, the BS is assumed to be in transmitting mode and the MS is assumed to be in receiving mode.
- The scatterer is assumed to be reflecting element with equal scattering coefficients and uniform random phases.
- The employed antennas are assumed to be isotropic for both the BS and MS.

The 3D spheroidal channel model's geometry and notations are shown in Figure 1. The spheroid is centered at the origin of the Global coordinate system O. The MS and BS are located on the x-axis at the spheroid's foci $(\pm f, 0, 0)$ and separated by a distance $D = 2f$, where f is the spheroid's focal length. The scatterers are uniformly distributed inside the spheroid's volume. However for graphical simplicity only one scatterer denoted by **S** is shown. The scatterer's Cartesian and Spherical coordinates with respect to the focal point are (x_m, y_m, z_m) and (r_m, θ_m, ϕ_m), respectively. The corresponding Cartesian coordinate with respect to the spheroid's center is (x_g, y_g, z_g). The transformation relationships between the two coordinate systems are given by

$$x_g = D/2 + x_m = D/2 + r_m \sin\theta_m \cos\phi_m, \tag{1}$$

$$y_g = y_m = r_m \sin\theta_m \sin\phi_m, \tag{2}$$

$$z_g = z_m = r_m \cos\theta_m. \tag{3}$$

Therefore, the spheroid can be described by the following formula

$$\frac{(D/2 + r_m \sin\theta_m \cos\phi_m)^2}{a^2} + \frac{r_m^2 \sin^2\theta_m \sin^2\phi_m + r_m^2 \cos^2\theta_m}{b^2} = 1.0, \tag{4}$$

where a and b are the spheroid's semi-lengths on the major axis, i.e., x-axis, and minor axes, i.e., y and z-axis, respectively. Solving for r_m results in a formula that is capable of describing the spheroid in the Spherical coordinate system as seen from its focal point. That is

$$r_m = \frac{2b^2}{(2a + D\sin\theta_m \cos\phi_m)}. \tag{5}$$

Similarly, due to the symmetry in the model's geometry, the radial distance as seen from the BS side, r_b, can be obtained as

$$r_b = \frac{2b^2}{(2a - D\sin\theta_b \cos\phi_b)}. \tag{6}$$

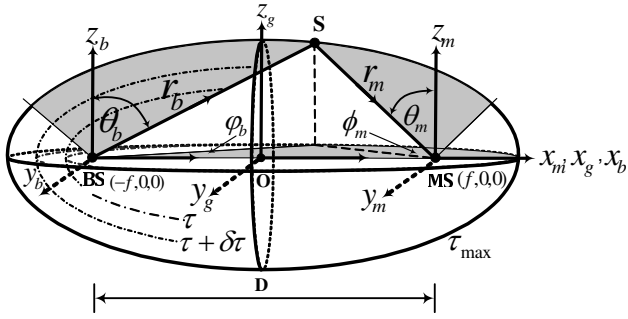

Figure 1. Spheroid model's geometry.

The total communication path length that results from a scatterer located on the spheroid's surface is given by

$$r_b + r_m = 2a = c\tau_{\max}, \tag{7}$$

where c is the speed of light and $\tau_{\max}$ is the maximum observation time. Thus, the model's parameters a and b may be expressed as

$$a = \frac{c\,\tau_{\max}}{2}, \tag{8}$$

$$b = \frac{\sqrt{c^2\tau_{\max}^2 - D^2}}{2}, \tag{9}$$

The spheroid's semi-lengths can be related as $b = a\sqrt{1-e^2}$ and the spheroid's eccentricity is defined as $e = D/2a$. Therefore, the radial distances, r_m and r_b, can be obtained as

$$r_m = \frac{c^2\tau_{\max}^2 - D^2}{2(c\tau_{\max} + D\sin\theta_m\cos\phi_m)}, \tag{10}$$

$$r_b = \frac{c^2\tau_{\max}^2 - D^2}{2(c\tau_{\max} - D\sin\theta_b\cos\phi_b)}, \tag{11}$$

where (θ_m, ϕ_m) and (θ_b, ϕ_b) are the AOA of the received multipath signals in the elevation and azimuth planes, as seen from the MS and BS, respectively. The AOA as seen from the BS can be considered as the angle of departure (AOD) of the transmitted signals.

3. ANGLE AND TIME OF ARRIVAL PROBABILITY DENSITY FUNCTIONS

The objective of this research work is to determine the AOA and TOA pdfs of the multipath signals, where the scatterers are assumed to be

uniformly distributed within the spheroid's volume and the BS and MS are located at the spheroid's foci.

3.1. Angle of Arrival Joint Probability Density Function

The AOA joint pdf, $f(\theta_m, \phi_m)$, of the received multipath signals can be obtained by determining the probability of the ith signal's arrival at the MS antenna within a certain range of AOA, (θ_m, ϕ_m), such that $0 < \theta_m^i \leq \theta_m$ and $0 < \phi_m^i \leq \phi_m$. As shown in Figure 1, all scatterers inside the spheroid cause multipath signals to arrive at the MS antenna at a TOA, τ, such that $\tau_o < \tau \leq \tau_{\max}$, where τ_o and $\tau_{\max}$ is the TOA of the line of sight (LOS) component and the maximum observation time respectively. Typically, $\tau_{\max}$ is determined according to available criteria based on desired channel characteristics [23]. The probability is obtained by normalizing the spheroid's slice, $V_{\tau_{\max}}(\theta_m, \phi_m)$, to the total volume of the spheroid, $V_{\tau_{\max}}$. These quantities are defined by

$$V_{\tau_{\max}}(\theta_m, \phi_m) = \int_0^{\phi_m} \int_0^{\theta_m} \frac{(c^2\tau_{\max}^2 - D^2)^3 \sin\alpha_m}{24(c\tau_{\max}^2 + D\sin\alpha_m \cos\beta_m)^3} d\alpha_m d\beta_m, \quad (12)$$

and

$$V_{\tau_{\max}} = \frac{\pi c\tau_{\max}(c^2{\tau_{\max}}^2 - D^2)}{6}. \quad (13)$$

Therefore, the probability of multipath components arriving at the MS within the specified range is given by

$$p_r(0 < \theta_m^i \leq \theta_m, 0 < \phi_m^i \leq \phi_m) = F(\theta_m, \phi_m)$$
$$= \int_0^{\phi_m} \int_0^{\theta_m} \frac{(c^2\tau_{\max}^2 - D^2)^2 \sin\alpha_m}{4\pi c\tau_{\max}(c\tau_{\max} + D\sin\alpha_m \cos\beta_m)^3} d\alpha_m d\beta_m, \quad (14)$$

where $F(\theta_m, \phi_m)$ is the AOA joint cumulative distribution function (CDF). Therefore the AOA joint pdf may be obtained as given by

$$f(\theta_m, \phi_m) = \frac{(c^2\tau_{\max}^2 - D^2)^2 \sin\theta_m}{4\pi c\tau_{\max}(c\tau_{\max} + D\sin\theta_m \cos\phi_m)^3},$$
$$0 < \theta_m \leq \pi, \quad 0 < \phi_m \leq 2\pi. \quad (15)$$

Similarly, due to the symmetry in the model's geometry, the AOA joint pdf at the BS can be obtained by using (11). This gives

$$f(\theta_b, \phi_b) = \frac{(c^2\tau_{\max}^2 - D^2)^2 \sin\theta_b}{4\pi c\tau_{\max}(c\tau_{\max} - D\sin\theta_b \cos\phi_b)^3},$$
$$0 < \theta_b \leq \pi, \quad 0 < \phi_b \leq 2\pi. \quad (16)$$

3.2. Angle of Arrival Joint Probability Density Function Conditioned on the Time of Arrival

The AOA joint pdf conditioned on the TOA of the multipath signals, $f(\theta_m, \phi_m|\tau)$, is determined based on the assumption that the scatterers are uniformly distributed within a 3D space that is limited by two spheroids corresponding to τ and $\tau + \delta\tau$ as shown in Figure 1. The normalization of the difference in volumes of the two spheroids' slices to the relative difference in their total volumes provides the probability for the multipath signals' arrival within specified AOA and TOA intervals, given as

$$\begin{aligned} & p(0 < \theta_m^i \le \theta_m\,,\, 0 < \phi_m^i \le \phi|\tau < \tau_i \le \tau + \delta\tau) = F(\theta_m, \phi_m|\tau) \\ = \; & \frac{V_{\tau+\delta\tau}(\theta_m, \phi_m) - V_\tau(\theta_m, \phi_m)}{V_{\tau+\delta\tau} - V_\tau}, \end{aligned} \tag{17}$$

where the volume of the spheroids' slices, i.e., $V_{\tau+\delta\tau}(\theta_m, \phi_m)$ and $V_\tau(\theta_m, \phi_m)$, and the total volume of the spheroids i.e., $V_{\tau+\delta\tau}$ and V_τ, can be obtained by using equations (12) and (13), respectively. Thus, dividing both the numerator and denominator of (17) by $\delta\tau$ and taking the limit when $\delta\tau$ goes to zero [23], results in

$$\begin{aligned} & p(0 < \theta_m^i \le \theta_m, 0 < \phi_m^i \le \phi|\tau < \tau_i \le \tau + \delta\tau) = \\ & \lim_{\delta\tau\to 0} \left(\frac{\left(\frac{V_{\tau+\delta\tau}(\theta_m,\phi_m) - V_\tau(\theta_m,\phi_m)}{\delta\tau} \right)}{\left(\frac{V_{\tau+\delta\tau} - V_\tau}{\delta\tau} \right)} \right) = \frac{\acute{V}_\tau(\theta_m, \phi_m)}{\acute{V}_\tau}, \end{aligned} \tag{18}$$

where $\acute{V}_\tau(\theta_m, \phi_m)$ and $\acute{V}_\tau$ are the derivations of the corresponding quantity with respect to τ. Substituting the derivations into (18) and simplifying, results in

$$\begin{aligned} & p(0 < \theta_m^i \le \theta_m\,,\, 0 < \phi_m^i \le \phi_m|\tau < \tau_i \le \tau + \delta\tau) \\ = \; & F(\theta_m, \phi_m|\tau) \int_0^{\phi_m} \int_0^{\theta_m} f(\alpha_m, \beta_m|\tau) d\alpha_m d\beta_m, \end{aligned} \tag{19}$$

where $f(\theta_m, \phi_m|\tau)$ is the AOA joint pdf conditioned on the TOA, which is given by

$$f(\theta_m, \phi_m|\tau) = \frac{3(c^2\tau^2 - D^2)^2(c^2\tau^2 + 2\,c\tau\, D \sin\theta_m \cos\phi_m + D^2) \sin\theta_m}{4\pi(3\,c^2\tau^2 - D^2)(c\tau + D\sin\theta_m \cos\phi_m)^4}. \tag{20}$$

Similarly, the AOA joint pdf conditioned on the TOA as seen from the BS is given as

$$f(\theta_b, \phi_b|\tau) = \frac{3(c^2\tau^2 - D^2)^2(c^2\tau^2 - 2c\tau D \sin\theta_b \cos\phi_b + D^2) \sin\theta_b}{4\pi\,(3\,c^2\tau^2 - D^2)(c\tau - D\sin\theta_b \cos\phi_b)^4}. \tag{21}$$

3.3. Angle and Time of Arrival Joint Probability Density Function

The scatterers are assumed to be uniformly distributed within the spheroid's volume based on the scatterers density model, $f(x_m, y_m, z_m)$, therefore, the AOA and TOA joint pdf, $f(\tau, \theta_m, \phi_m)$, can be obtained by making use of the Jacobian transformation. This gives

$$f(r_m, \theta_m, \phi_m) = r_m^2 \sin\theta_m f(x_m, y_m, z_m). \tag{22}$$

where the Jacobian transformation, $J(x_m, y_m, z_m)$, is given by $1/r_m^2 \sin\theta_m$. The TOA variable can be included in order to determine the AOA and TOA joint pdfs, $f(\tau, \theta_m, \phi_m)$, of the multipath signals as seen from the MS as gives by

$$f(\tau, \theta_m, \phi_m) = \left. \frac{r_m^2 \sin\theta_m f(x_m, y_m, z_m)}{|J(r_m, \theta_m, \phi_m)|} \right|_{r_m = \frac{(c^2\tau^2 - D^2)}{2(c\tau + D\sin\theta_m \cos\phi_m)}}, \tag{23}$$

where the Jacobian transformation $J(r_m, \theta_m, \phi_m)$ is given by

$$J(r_m, \theta_m, \phi_m) = \frac{2(c\tau + D\sin\theta_m \cos\phi_m)^2}{c(c^2\tau^2 + 2c\tau D\sin\theta_m \cos\phi_m + D^2)}. \tag{24}$$

Substituting (24) into (23) and simplifying results in an AOA and TOA joint pdf for a given scatterers density function, $f(x_m, y_m, z_m)$, as given by

$$f(\tau, \theta_m, \phi_m) = \frac{c\left(c^2\tau^2 - D^2\right)^2 \left(c^2\tau^2 + 2c\tau D\sin\theta_m \cos\phi_m + D^2\right) \sin\theta_m}{8\left(c\tau + D\sin\theta_m \cos\phi_m\right)^4} \times f(x_m, y_m, z_m). \tag{25}$$

The derived joint pdf is applicable to any distribution of scatterers around the MS. For example, as shown in Figure 1, the scatterers are assumed to be uniformly distributed within the spheroid's volume, where the spheroid's volume is limited by $\tau_{\max}$. In this case, the scatterers density function, $f(x_m, y_m, z_m)$, is given by $1/V_{\tau_{\max}}$, the scatterers density function can then be obtained as

$$f(x_m, y_m, z_m) = \frac{6}{\pi c \tau_{\max}(c^2 {\tau_{\max}}^2 - D^2)}. \tag{26}$$

Substituting (26) into (25), results in the AOA and TOA joint pdf of the multipath signals as seen from the MS. Thus

$$f(\tau, \theta_m, \phi_m) = \frac{3\left(c^2\tau^2 - D^2\right)^2 \left(c^2\tau^2 + 2c\tau D\sin\ \theta_m \cos\phi_m + D^2\right) \sin\theta_m}{4\pi\tau_{\max}(c^2 {\tau_{\max}}^2 - D^2)\left(c\tau + D\sin\theta_m \cos\phi_m\right)^4}, \tag{27}$$

which is equivalent to $f(\theta_m, \phi_m/\tau) \times f(\tau)$ which are given by (20) and (32) respectively. (Note: the TOA marginal pdf, $f(\tau)$, is derived in Section 3.5).

3.4. Angle and Time of Arrival Joint Probability Density Function for an Elevated Base Station

In some outdoor and indoor wireless communication scenarios, the BS antennas are elevated in comparison to the MS antennas. To include the antennas' relative difference in height, the spheroid model's geometry can be inclined as shown in Figure 2, where α is the inclination angle, which is given by

$$\alpha = \tan^{-1}\left(\frac{H_{BS} - H_{MS}}{D}\right), \tag{28}$$

where H_{BS} and H_{MS} are the heights of the BS and MS antennas, respectively. In such a case, the radial distance, r_m, can be derived as

$$r_m = \frac{c^2\tau_{\max}^2 - D^2}{2(c\tau_{\max} + D(\sin\theta_m \cos\phi_m \cos\alpha - \sin\theta_m \sin\alpha)}. \tag{29}$$

Therefore, all derived AOA pdfs can be modified to include the difference in heights between the BS and MS. For example, the AOA joint pdf at the MS may be given by

$$f(\theta_m, \phi_m) = \frac{(c^2\tau_{\max}^2 - D^2)^2 \sin\theta_m}{4\pi c\tau_{\max}(c\tau_{\max} + D(\sin\theta_m \cos\phi_m \cos\alpha - \sin\theta_m \sin\alpha))^3}. \tag{30}$$

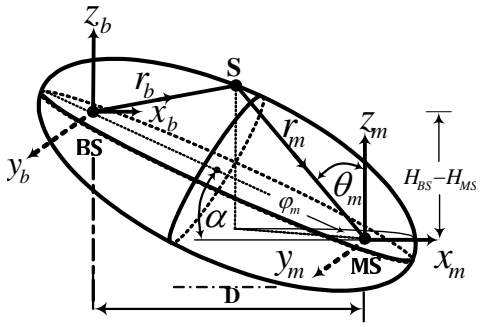

Figure 2. Elevated BS model's geometry.

3.5. Time of Arrival Marginal Probability Density Function

The probability that the multipath components arrive with a delay τ, such that $\tau_o < \tau \leq \tau_{\max}$ can be obtained by normalizing the volume V_τ to the volume $V_{\tau_{\max}}$, where τ is TOA of the multipath signals. As shown in Figure 1, these volumes, V_τ and $V_{\tau_{\max}}$, are defined as the volume of the spheroid which encloses the scatterers that cause multipath signals to arrive before τ and $\tau_{\max}$ respectively. These quantities, i.e., V_τ and $V_{\tau_{\max}}$, can be obtained by using Equation (13). Therefore, normalizing the mentioned volumes, results in

$$p_r(\tau_o < \tau \leq \tau_{\max}) = F(\tau) = \frac{\tau\,(c^2\tau^2 - D^2)}{\tau_{\max}(c^2{\tau_{\max}}^2 - D^2)}, \tag{31}$$

where $F(\tau)$ is the TOA marginal CDF. Differentiating (31) with respect to τ results in the TOA marginal pdf as follows

$$f(\tau) = \frac{3\,c^2\tau^2 - D^2}{\tau_{\max}\,(c^2{\tau_{\max}}^2 - D^2)} \qquad \tau_o < \tau \leq \tau_{\max}. \tag{32}$$

4. NUMERICAL RESULTS AND MODEL'S COMPARISONS

To illustrate and verify the developed 3D model, several numerical 2D and 3D results are provided for the AOA and TOA pdfs. To make comparisons easier, all plots for the pdfs have been normalized for their maximum values. Figure 3(a) and Figure 3(b) show the 3D graph of the AOA joint pdfs at the MS, $f(\theta_m, \phi_m)$, and BS, $f(\theta_b, \phi_b)$, respectively, for $\tau = 1.5\tau_o$, where τ_o is the TOA of the LOS component. It is clear that the most frequent occurrences of the AOA take place around the relative direction between the MS and BS in both the elevation angle, $\theta_m = 90°$, and azimuth angle, $\phi_m = 180°$ and $\phi_b = 0°$.

To verify the AOA and TOA expressions, they have been compared with histograms of simulated pdfs. The histograms were created by simulating 10^5 scatterers uniformly distributed within the spheroid's volume, where the spheroid's semi-lengths were the same as those used in plotting the theoretical pdfs. As such, for all scatterers, the desired AOA and TOA of the multipath signals were calculated based on the locations of the scatterers, the MS and the BS. A histogram containing 50 bins (intervals) was then created and the number of points in each bin was normalized to the total number of points.

Figure 4(a) and Figure 4(b) show the plots of the theoretical and simulated AOA pdfs in the azimuth angle, $f(\phi_m)$, and BS, $f(\phi_b)$, respectively, and the plot of the AOA pdf in the elevation angle,

$f(\theta_m)$, is shown in Figure 4(c). The pdfs have been illustrated for various values of maximum observation time, $\tau_{\max} = 1.5\tau_o, 2.0\tau_o$, and $3.0\tau_o$. These figures illustrate that the angular spread in the azimuth

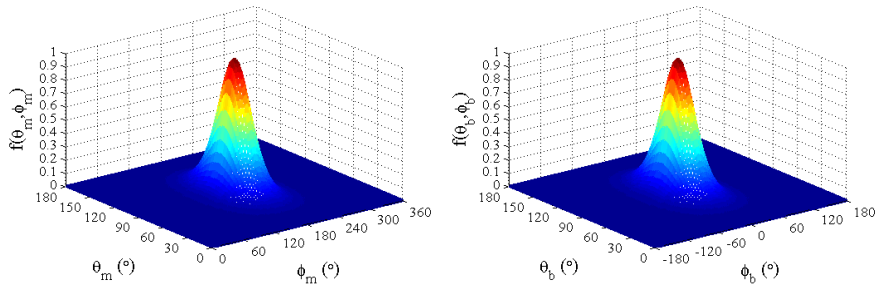

(a) $f(\theta_m, \phi_m)$ (b) $f(\theta_b, \phi_b)$

Figure 3. The AOA joint pdfs at the MS and BS for $\tau_{\max} = 1.5\tau_o$

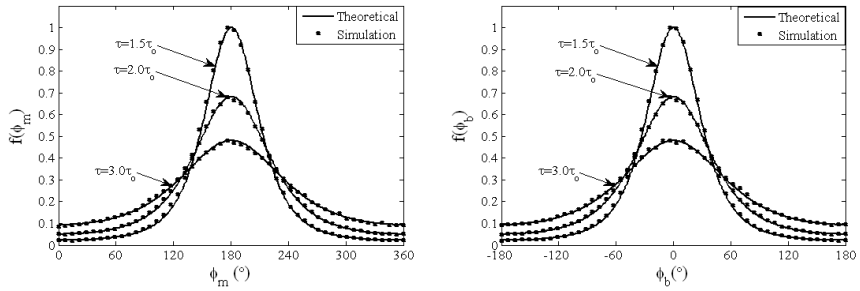

(a) $f(\phi_m)$ (b) $f(\phi_b)$

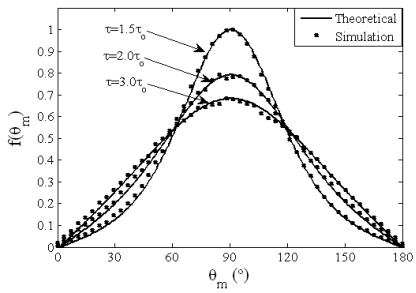

(c) $f(\theta_m)$

Figure 4. The AOA marginal pdfs in the azimuth and elevation angle as seen from the MS and BS for $\tau_{\max} = 1.5, 2.0$, and $3.0\tau_o$.

and elevation planes increase when the maximum observation time is increased. In other words, the azimuthal and elevational angular spread depends upon the maximum observation time value at a fixed separation distance. Consistent agreement between the theoretical and simulated graphs is clearly illustrated in all the AOA pdfs.

Figure 5(a) and Figure 5(b) illustrate the 3D plots of the AOA and TOA joint pdfs in the azimuth angle, $f(\tau, \phi_m)$, and elevation angle, $f(\tau, \theta_m)$, respectively, for $\tau_{\max} = 5\tau_o$. It is clear that by increasing the maximum observation time, $\tau_{\max}$, the AOA distribution in the azimuth angle approaches a uniform distribution, $f(\phi_m) = 1/2\pi$, and the AOA distribution in the elevation angle approaches a sinusoidal distribution, $f(\theta_m) = \sin(\theta_m)$. These results agree with the azimuthal and elevational angular distributions when the scatterers are assumed to be uniformly distributed within a sphere, as the spheroid geometry can approximate a sphere for large values of $\tau_{\max}$.

Figure 6 shows the AOA pdf for different inclination angles, $\alpha = 0°$, $10°$, $20°$ and $30°$, for the separation distance $D = 30$ m, which results in 0, 5, 10 and 15 m of difference in the BS and MS antennas' heights, respectively. It is clearly shown that the most frequent AOAs are around $\theta_m = 90°$, $80°$, $70°$ and $60°$ for $\alpha = 0°$, $10°$, $20°$,and $30°$ respectively. Figure 7 shows the plot of the marginal TOA pdf as a function of the normalized TOA, τ/τ_o, for $\tau_{\max} = 3.0\tau_o$. As shown, the graph increases with an increase in the TOA.

To validate the developed geometrical scattering channel model, the model has been compared against similar 2D models. For example, the AOA marginal and conditioned pdfs as seen from the MS have been proposed based on the 2D elliptical model [1], i.e., $\theta_m = 90°$, where the elliptical model is generalized in [3] to obtain the marginal pdfs as seen from both the MS and BS. The developed 3D spheroid model can

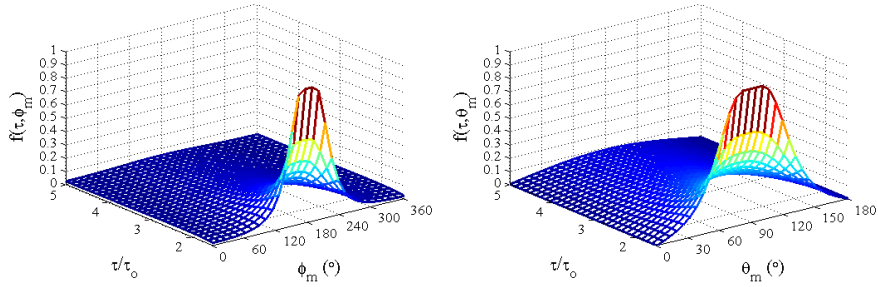

(a) $f(\tau, \phi_m)$ (b) $f(\tau, \theta_m)$

Figure 5. The AOA and TOA joint pdfs at the MS for $\tau_{\max} = 5\tau_o$.

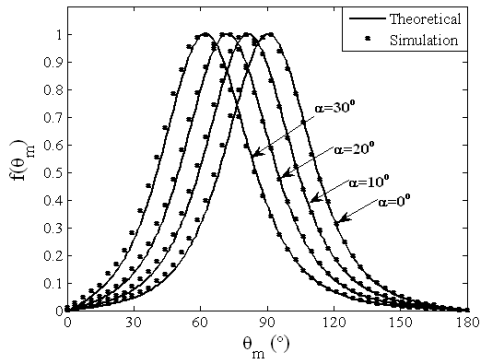

Figure 6. The AOA pdf at the MS $f(\theta_m)$ for $\alpha = 0°$, $10°$, $20°$ and $30°$.

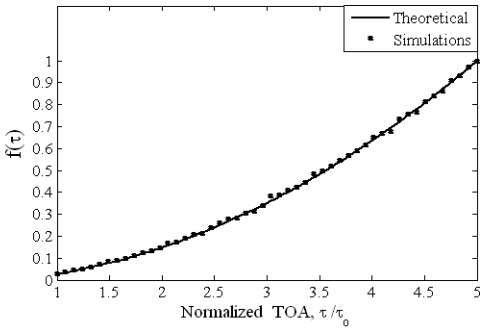

Figure 7. The TOA pdf, $f(\tau)$, in terms of the normalized TOA, τ/τ_o.

be reduced to obtain the AOA pdfs in the azimuth plane that have been derived based on the 2D models, as shown

$$f(\phi_m)_{2D} = \left. \frac{f(\theta_m, \phi_m)_{3D}}{\int_0^{2\pi} f(\theta_m, \phi_m)_{3D} d\phi_m} \right|_{\theta_m = 90°,} \tag{33}$$

$$f(\phi_m/\tau)_{2D} = \left. \frac{f(\theta_m, \phi_m|\tau)_{3D}}{\int_0^{2\pi} f(\theta_m, \phi_m|\tau)_{3D} d\phi_m} \right|_{\theta_m = 90°.} \tag{34}$$

Figure 8(a) and Figure 8(c) illustrate the comparisons of the AOA marginal and conditioned pdfs that have been determined based on the proposed 3D spheroid model and Liberti's 2D model [1]. Similarly,

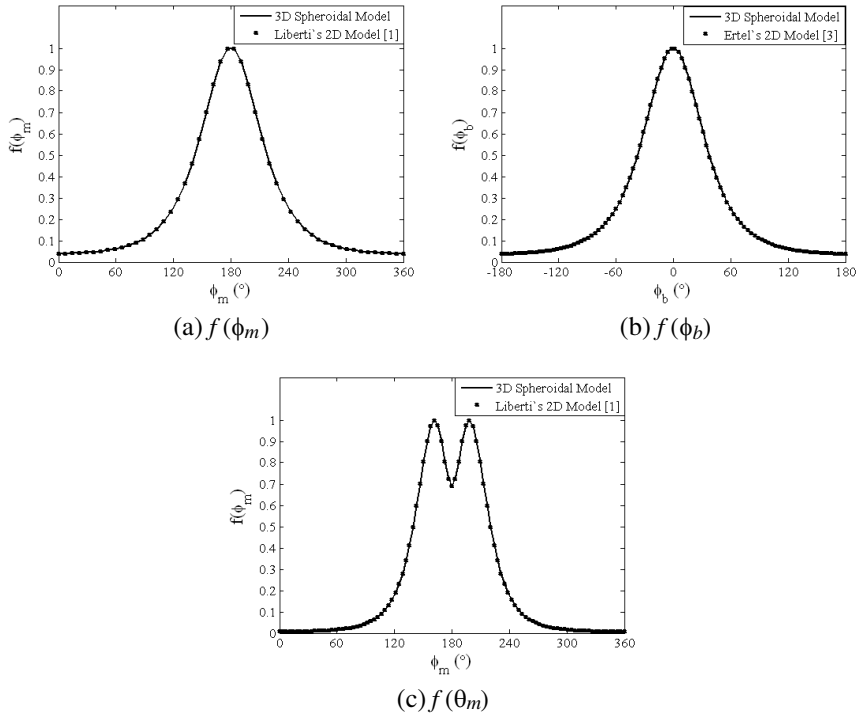

Figure 8. Comparison of AOA pdf in the azimuth angle with the Liberti's [1] and Ertel's [3] 2D models.

comparisons of the AOA marginal pdf, as seen from the BS, with Ertel's 2D model [3] is illustrated in Figure 8(b). All plots illustrate strong agreement between the proposed 3D model and the similar 2D models. Furthermore, the model has been compared against the validated 2D geometrical scattering channel models [4, 8, 9]. These 2D models have been validated by comparing their AOA pdf in the azimuth angle with some of the available measured data [24–26]. The derived AOA joint pdf as seen from the BS can be obtain by

$$f(\phi_b)_{2D} = \left. \frac{f(\theta_b, \phi_b)_{3D}}{\int_0^{2\pi} f(\theta_b, \phi_b)_{3D} d\phi_b} \right|_{\theta_b = 90^\circ,} \tag{35}$$

where $f(\theta_b, \phi_b)$ is the AOA joint pdf as seen from the BS, which is given by

$$f(\theta_b, \phi_b) = \frac{(1 - e^2)^2 \sin\theta_b}{4\pi(1 - e\sin\theta_b \cos\phi_b)^3}. \tag{36}$$

The measured root mean square (RMS) angular spreads, i.e., standard deviation, can be used in extracting the physical model's parameters, i.e., spheroid's eccentricity, to produce similar results. The theoretical RMS angular spread can be calculated as

$$\sigma_{\phi_b} = \sqrt{E[\phi_b^2] - E[\phi_b]^2}, \tag{37}$$

where $E[\phi_b]$ and $E[\phi_b^2]$ are the mean, μ_{ϕ_b}, and the second moment of the random variable ϕ_b, respectively. These quantities can be determined from their usual definitions

$$E[\phi_b] = \int_{-\pi}^{\pi} \phi_b f(\phi_b) d\phi_b, \tag{38}$$

$$E[\phi_b^2] = \int_{-\pi}^{\pi} \phi_b^2 f(\phi_b) d\phi_b. \tag{39}$$

The plot of the RMS angular spread in the azimuth angle, σ_{ϕ_b}, versus the spheroid's eccentricity, e, is shown in Figure 9. Pedersen et al. in [24], conducted outdoor channel measurements at the urban areas of Aarhus, Denmark and Stockholm, Sweden. Wideband measurements were conducted at a carrier frequency of 1.8 GHz and at a sampling time of 122 ns. The measured angular data had a standard deviation of 6°. Spencer et al. in [25], conducted indoor channel measurements within office buildings in the Brigham Young University (BYU) campus. The data was collected at 7 GHz in the angle and time domains with impulse response measurements carried out using a narrow-beam dish antenna. The AOA measurements had a standard deviation in angle of 24.5°. Cramer et al. in [26], collected data in an office/laboratory building. In the experiment, the location of the transmitting antenna is fixed, and rectangular arrays of measurements are made by moving the receiving antenna to 49 points in a 7×7 array. They showed that the relative arrival in the azimuth arrival angles of the recovered ultra-wideband signals gave the best fit for a Laplacian distribution, with a standard deviation of 38°. Accordingly, as shown in Figure 9, values of $e = 0.99$, 0.88 and 0.76 is required to produce standard deviation of 6°, 24.4° and 38° respectively, where $e = D/2a$. As shown in Figure 10, the comparisons of the derived AOA pdfs in the azimuth angle with the 2D geometrical scatterering channel models and the corresponding measured channel data are provided. As illustrated, comparisons' results show good agreement between the proposed 3D model and the 2D models as well as the measured data. A log scale has been used in Figure 10(b) and Figure 10(c) to permit easier comparisons [4] and [9].

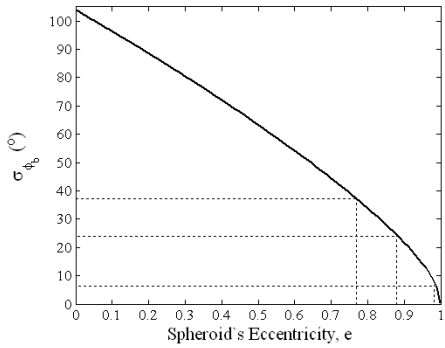

Figure 9. RMS angular spread, σ_{ϕ_b}, versus spheroid's eccentricity, e.

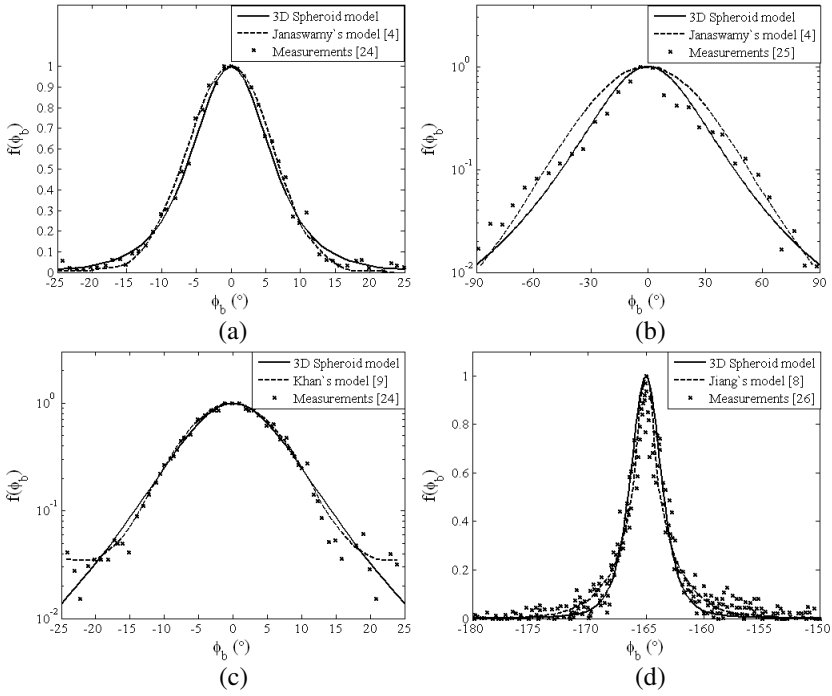

Figure 10. Comparison of AOA expression in the azimuth angle with: (a) Janaswamy's 2D model [4] and measurements [22], (b) Janaswamy's model [4] and measurements [25], (c) Khan's model [9] and measurements [24] and (d) Jiang's model [8] and measurements [26].

5. CONCLUSION

In this paper, a 3D geometrical scattering channel model has been introduced. The model is based on the assumption that all significant scatterers are uniformly distributed within a spheroid's volume in which the BS and MS are located at it's foci. The model provides both the spatial and temporal statistical information of the received multipath signals. Closed form pdfs for the AOA and TOA, as seen from both the MS and BS are provided. Several numerical results are presented to illustrate and verify the derived expressions. To establish the model's validation, the model has been compared against some available 2D models and measured data. Comparisons results illustrate good agreement between the proposed 3D model and the 2D models as well as the measured data. The introduced 3D model is useful in wireless communication environments, in which the most frequent occurrences of the AOA of the received multipath signals take place around the relative direction of the BS to the MS in both the azimuth and the elevation angles, such as in outdoor picocellular and indoor propagation environments.

REFERENCES

1. Liberti, J. C. and T. S. Rappaport, "A geometrically based model for line of sight multipath radio channels," *IEEE Vehicular Technology Conf.*, 844–848, Apr. 1996.
2. Norklit, O. and J. Andersen, "Diffuse channel model and experimental results for array antennas in mobile environments," *IEEE Trans. Antennas and Propagt.*, Vol. 46, No. 6, 834–843, Jun. 1998.
3. Ertel, R. B. and J. H. Reed, "Angle and time of arrival statistics for circular and elliptical scattering models," *IEEE J. Sel. Areas Commun.*, Vol. 17, 1829–1840, Nov. 1999.
4. Janaswamy, R., "Angle and time of arrival statistics for the Gaussian scatter density model," *IEEE Trans. Wireless Commun.*, Vol. 1, 488–497, Jul. 2002.
5. Petrus, P., J. Reed, and T. Rappaport, "Geometrical-based statistical macrocell channel model for mobile environments," *IEEE Trans. Commun.*, Vol. 50, No. 3, 495–502, Mar. 2002.
6. Olenko, A., K. Wong, and M. Abdulla, "Analytically derived TOA-DOA distributions of uplink/downlink wireless-cellular multipaths arisen from scatterers with an inverted-parabolic

spatial distribution around the mobile," *IEEE Signal Processing Letters*, Vol. 12, No. 7, 516–519, Jul. 2005.

7. Imai, T. and T. Taga, "Statistical scattering model in urban propagation environment," *IEEE Trans. Veh. Technol.*, Vol. 55, No. 4, 1081–1093, Jul. 2006.
8. Jiang, L. and S. Y. Tan, "Geometrically based statistical channel models for outdoor and indoor propagation environments," *IEEE Trans. Veh. Technol.*, Vol. 56, No. 6, 3587–3593, Nov. 2007.
9. Khan, N. M., M. T. Simsim, and P. B. Rapajic, "A generalized model for the spatial characteristics of the cellular mobile channel," *IEEE Trans. Veh. Technol.*, Vol. 57, No. 1, 22–37, Jan. 2008.
10. Mahmoud, S. S., F. S. Al-Qahtani, Z. M. Hussain, and A. Gopalakrishnan, "Spatial and temporal statistics for the geometrical-based hyperbolic macrocell channel model," *Digital Signal Processing*, Vol. 18, No. 2, 151–167, Mar. 2008.
11. Le, K. N., "On angle-of-arrival and time-of-arrival statistics of geometric scattering channels," *IEEE Trans. on Veh. Technol.*, Vol. 58, No. 8, 4257–4264, Oct. 2009.
12. Chen, Y., Z. Zhang, L. Hu, and P. Rapajic, "Geometry-based statistical model for radio propagation in rectangular office buildings," *Progress In Electromagnetics Research B*, Vol. 17, 187–212, 2009.
13. Chen, Y., Z. Zhang, and T. Qin, "Geometrically based channel model for indoor radio propagation with directional antennas," *Progress In Electromagnetics Research B*, Vol. 20, 109–124, 2010.
14. Janaswamy, R., "Angle of arrival statistics for a 3D spheroid model," *IEEE Trans. Veh. Technol.*, Vol. 51, No. 5, 1242–1247, Sep. 2002.
15. Olenko, A. Y., K. T. Wong, S. A. Qasmi, and J. Ahmadi-Shokouh, "Analytically derived uplink/downlink TOA and 2D DOA distributions with scatterers in a 3D hemispheroid surrounding the mobile," *IEEE Trans. Antennas Propagat.*, Vol. 54, No. 9, 2446–2454, Sep. 2006.
16. Baltzis, K. B. and J. N. Sahalos, "A simple 3D geometric channel model for macrocell mobile communication," *Wireless Pers. Commun.*, Vol. 51, No. 2, 329–347, Oct. 2008.
17. Nawaz, S. J., B. H. Qureshi, and N. M. Khan, "A generalized 3D scattering model for macrocell environment with directional antenna at BS," *IEEE Trans. Veh. Technol.*, Vol. 59, No. 7, 3193–3204, Sep. 2010.

18. Fuhl, J., J. P. Rossi, and E. Bonek, "High-resolution 3D direction-of-arrival determination for urban mobile radio," *IEEE Trans. Antennas Propagat.*, Vol. 45, 672–682, Apr. 1997.
19. Kuchar, A., J. P. Rossi, and E. Bonek, "Directional macro-cell channel characterization from urban measurements," *IEEE Trans. Antennas Propagt.*, Vol. 48, No. 2, 137–146, 2000.
20. Laurila, J., K. Kalliola, M. Toeltsch, K. Hugl, P. Vainikainen, and E. Bonek, "Wide-band 3D characterization of mobile radio channels in urban environment," *IEEE Trans. Antennas Propagt.*, Vol. 50, No. 2, 233–243, Feb. 2002.
21. Kalliola, K., H. Laitinen, P. Vainikainen, M. Toeltsch, J. Laurila, and E. Bonek, "3D double-directional radio channel characterization for urban macrocellular applications," *IEEE Trans. Antenna and Propagat.*, Vol. 51, No. 11, 3122–3133, Nov. 2003.
22. Gurrieri, L. E., T. J. Willink, A. Petosa, and S. Noghanian, "Characterization of the angle, delay and polarization of multipath signals for indoor environments," *IEEE Trans. Antennas Propagat.*, Vol. 56, No. 8, 2710–2719, Aug. 2008.
23. Liberti, J. C. and T. S. Rappaport, *Smart Antennas for Wireless Communcations: IS-95 and Third Generation CDMA Applications*, Prentice Hall, 1999.
24. Pedersen, K. I., "A stochastic model of the temporal and azimuthal dispersion seen at the base station in outdoor propagation environments," *IEEE Trans. Veh. Technol.*, Vol. 49, 437–447, Mar. 2000.
25. Spencer, Q. H., B. D. Jeffs, M. A. Jensen, and A. L. Swindlehurst, "Modeling the statistical time and angle of arrival characteristics of an indoor multipath channel," *IEEE J. Sel. Areas Commun.*, Vol. 18, No. 3, 347–360, Mar. 2000.
26. Cramer, R. J.-M., R. A. Scholtz, and M. Z. Win, "Evaluation of an ultrawideband propagation channel," *IEEE Trans. Antennas Propagt.*, Vol. 50, No. 5, 561–570, May 2002.